Benefits and Limitations of High-Resolution Cyclic IM-MS for Conformational Characterization of Native Therapeutic Monoclonal Antibodies

Evolène Deslignière, Simon Ollivier, Alain Beck, David Ropartz, Hélène Rogniaux, Sarah Cianférani

Benefits and Limitations of High-Resolution Cyclic IM-MS for Conformational Characterization of Native Therapeutic Monoclonal Antibodies

Evolène Deslignière[1,2¶], Simon Ollivier[3,4,¶], Alain Beck[5], David Ropartz[3,4], Hélène Rogniaux[3,4], Sarah Cianférani[1,2,*]

[1] Laboratoire de Spectrométrie de Masse BioOrganique, IPHC UMR 7178, Université de Strasbourg, CNRS, 67000 Strasbourg, France

[2] Infrastructure Nationale de Protéomique ProFI – FR2048, 67087 Strasbourg, France

[3] INRAE, UR BIA, F-44316 Nantes, France

[4] INRAE, PROBE Research Infrastructure, BIBS Facility, F-44316 Nantes, France

[5] IRPF Centre d'Immunologie Pierre-Fabre (CIPF), 74160 Saint-Julien-en-Genevois, France

*Corresponding author: sarah.cianferani@unistra.fr

ABSTRACT

Monoclonal antibodies (mAbs) currently represent the main class of therapeutic proteins. MAbs approved by regulatory agencies are selected from IgG1, IgG2, and IgG4 subclasses, which possess different interchain disulfide connectivities. Ion mobility coupled to native mass spectrometry (IM-MS) has emerged as a valuable approach to tackle the challenging characterization of mAbs' higher order structures. However, due to the limited resolution of first-generation IM-MS instruments, subtle conformational differences on large proteins have long been hard to capture. Recent technological developments have aimed at increasing available IM resolving powers and acquisition mode capabilities, namely through the release of high-resolution IM-MS (HR-IM-MS) instruments, like cyclic IM-MS (cIM-MS). Here, we outline the advantages and drawbacks of cIM-MS for better conformational characterization of intact mAbs (~150 kDa) in native conditions compared to first-generation instruments. We first assessed the extent to which multipass cIM-MS experiments could improve the separation of mAbs' conformers. These initial results evidenced some limitations of HR-IM-MS for large native biomolecules which possess rich conformational landscapes that remain challenging to decipher even with higher IM resolving powers. Conversely, for collision-induced unfolding (CIU) approaches, higher resolution proved to be particularly useful (i) to reveal new unfolding states, and (ii) to enhance the separation of coexisting activated states, thus allowing to apprehend gas-phase CIU behaviors of mAbs directly at the intact level. Altogether, this study offers a first panoramic overview of the capabilities of cIM-MS for therapeutic mAbs, paving the way for more widespread HR-IM-MS/CIU characterization of mAb-derived formats.

INTRODUCTION

Monoclonal antibodies (mAbs) and their derived formats constitute the fastest growing class of therapeutic agents against several diseases, including cancers or neurodegenerative disorders[1]. Approved antibody products are selected from three immunoglobulin (IgG) subclasses, IgG1, IgG2, and IgG4, which exhibit different numbers or patterns of interchain disulfide bonds in the hinge region[2]. IgGs present significant regulatory challenges compared to small molecules because of their size (~150 kDa), their intrinsic heterogeneity resulting from post-translational modifications (PTMs) superimposed to an additional level of complexity related to drug conjugation for antibody-drug conjugates (ADCs)[3]. As alterations in higher order structures (HOS) can influence the immunogenicity and biological activity of mAbs, a thorough characterization of mAbs' HOS is crucial to ensure the stability, safety, and efficacy of biotherapeutics along drug product development[3]. The coupling of ion mobility to native mass spectrometry (IM-MS) is particularly interesting to analyze HOS in a rapid manner[4]. IM separates ions based on their size, shape, and charge. The resulting arrival time distribution (ATD) provides information on conformational heterogeneity/homogeneity. Arrival times may be further converted into rotationally averaged collision cross sections (CCS, Ω) which reflect the three-dimensional conformations of ions in the gas phase. Native IM-MS has been used for the study of the NIST mAb[5], to assess the influence of mAb (de)glycosylation[6], to monitor Fab-arm exchange and bispecific antibody formation[7], for forced degradation studies[8], or to measure drug-to-antibody ratio of ADCs[9-11]. Native IM-MS thus appears as an attractive technique for the study of biopharmaceuticals, but it is still yet to gain popularity in industry[12].

Full high-resolution structural characterization of mAbs using electron microscopy or crystallography has been hindered by their dynamic and highly flexible nature (due to Fab arm waving/rotation, Fab elbow bending, Fc wagging[13]), which is well reflected by the few full length IgG structures deposited in the protein data bank (PDB)[14-18]. Hence, low-resolution techniques are still desired to investigate HOS of mAbs. Because of mAbs' dynamics, subtle differences in mAb conformations have eluded IM-MS measurements[9, 10, 19, 20], and so variable-temperature IM-MS has been proposed to reduce structural flexibility by working at lower temperatures[21, 22]. Besides, mAbs are quasi iso-cross sectional, and so first-generation traveling wave IM spectrometry (TWIMS) instruments find limited applications for mAb conformational characterization at intact level, because of a limited resolving power (R ~40 $\Omega/\Delta\Omega$)[23]. Over the last years, different high-resolution IM-MS (HR-IM-MS) technologies have thus been developed, among which structures for lossless manipulations (SLIM)[24], trapped IM spectrometry (TIMS)[25], and cyclic TWIMS (cIM)[26]. The latest generation of cIM-MS instruments, which comprises a ~1-m cyclic cell placed orthogonally to the main ion optical axis, affords an enhanced resolution using multipass separation (R ~750 after 100 passes), and the possibility to perform tandem IM/IM experiments[26]. Despite these advancements towards higher IM resolving powers, several groups have shown that it remains difficult to separate coexisting/interconverting conformations of native proteins[27-29]. Collision-induced unfolding (CIU) approaches represent an appealing alternative when even high-resolution IM-MS measurements fail to distinguish closely related conformations[30]. CIU consists of activating ions through collisions with background gas prior to IM separation, allowing to monitor protein

folding/unfolding with IM and to differentiate proteins based on their gas-phase behaviors. CIU has proved to be a powerful tool for the characterization of therapeutic mAb formats[19, 31-33], and was applied to concrete challenges encountered in the biopharmaceutical industry, including Fab-arm exchange[34], differentiation of wild-type *versus* hinge-stabilized IgG4s[19], and multispecific formats[35], or even to pinpoint the hybridicity of eculizumab (IgG2/4) based on subdomains' fingerprints[20].

While we have previously reported on the interest of using cIM-MS in a real case scenario for the separation of cis/trans isomers from a trispecific antibody under development[35], the aim of the present work is to provide a more general and extensive study on the benefits and limitations of cIM-MS for a detailed conformational characterization of native intact mAbs compared to first-generation instruments. We focused here on two aspects: (i) the potential gain in resolution afforded by cIM-MS to enhance the separation of mAbs' conformers, and (ii) the impact of higher IM resolving powers for CIU experiments. As disulfide-bonded proteins are known to be well adapted for IM-MS and CIU-based studies[20, 31, 36-39], we then used IgG subclassification as a fit for purpose application to benchmark cyclic *versus* linear TWIMS instruments. We show that increasing the resolution with multiple passes in the cIM cell affords only limited improvements for the direct measurement of ATDs of native mAbs because an intrinsic peak broadening occurs, presumably related to the coexistence of several protein conformations that lead to a nearly continuous range of CCSs. Conversely, CIU experiments clearly benefit from higher resolution, as new states are uncovered upon activation, along with a better separation of activated features, leading to a more comprehensive characterization of the gas-phase behaviors of mAbs and their different subclasses. Overall, our study gives an overview of advantages and drawbacks of HR IM-MS and CIU approaches to probe mAbs' HOS, paving the way for more widespread application of the cIM-MS technology for biotherapeutics.

EXPERIMENTAL SECTION

Sample preparation. Elotuzumab (IgG1, Empliciti, BMS), ofatumumab (IgG1, Arzerra, GSK), trastuzumab (IgG1, Herceptin, Roche), denosumab (IgG2, Prolia/Xgeva, Amgen), panitumumab (IgG2, Vectibix, Amgen), eculizumab (IgG2/4, Solaris, Alexion Pharmaceuticals Inc.), natalizumab (IgG4, Tysabri, Biogen), nivolumab (IgG4, Opdivo, BMS), and reslizumab (IgG4, Cinqair, Teva), were obtained from their respective manufacturers. Of note, the hybrid eculizumab (IgG2/4) has IgG2-like hinge disulfide bonds, and has been shown to behave like an IgG2 at the intact level as a result of IM behaviors being driven by interchain disulfide bonds[20]. In order to obtain more homogeneous native mass spectra, each mAb was N-deglycosylated by incubating one unit of IgGZERO (Genovis) per microgram of mAb for 30 min at 37°C.

Buffer exchange. Samples were desalted against 100 mM ammonium acetate at pH 6.9, using six cycles of centrifugal concentrator (Vivaspin, 50 kDa cutoff, Sartorius, Göttingen, Germany). Protein concentration was determined by UV absorbance using a NanoDrop spectrophotometer (Thermo Fisher

Scientific, France). Each sample was diluted to 7 µM in 100 mM ammonium acetate at pH 6.9 prior to native (IM)-MS analysis.

Native IM-MS on the linear TWIMS instrument. Experiments were carried out using direct ESI injection on a Z-spray ion source. The Synapt G2 HDMS mass spectrometer (Waters, Wilmslow, U.K.) was operated in sensitivity mode and positive polarity using a capillary voltage of 3.0 kV. Desolvation and cone gas flow rates were 750 and 60 L/Hr, respectively. Desolvation and source temperatures were fixed to 250 and 50°C, respectively. In order to minimize in-source activation while ensuring ion transmission, the cone voltage was set to 80 V. The pressure in the interface region was 6 mbar. The argon flow rate was 5 mL/min. Ions were focused in the helium cell (120 mL/min) before IM separation. The nitrogen flow rate was 60 mL/min in the linear TWIMS cell. The IM wave velocity and height were fixed to 800 m/s and 40 V, respectively. Data were acquired in the 1000 – 10,000 *m/z* range.

Native MS and IM-MS on the cyclic TWIMS instrument. Acquisitions were performed through direct ESI injection (on a Z-spray ion source equipped with a low flow ESI probe) on a SELECT SERIES Cyclic IMS (Waters, Wilmslow, U.K.) in the *m/z* range 50 – 8000. Samples were analyzed in positive ion mode, with the following parameters: capillary 1.8 kV; sampling cone 80 V; source offset 30 V; source temperature 50 °C; desolvation temperature 250 °C. The pressure in the interface region was 2.6 mbar. cIM experiments were carried out in N60 purity nitrogen (Alphagaz 2, Air Liquide, France), at a pressure of 1.7 mbar. Wave velocity and height were set to 900 m/s and 45 V, respectively. Ions were ejected from the cIM racetrack with a forward traveling wave of 600 m/s. In order to work on native proteins, voltages in the multifunction array region, which allows to perform fine manipulation of the ion populations during IM and IM^n experiments, were modified as described in Table S1.

Data treatment and Gaussian fitting. IM data were analyzed with MassLynx v4.3 (Waters, Milford, MA, USA). Raw arrival times t_A were converted into drift times t_D by subtracting the IM injection time and the time ions spend traveling from the array to the ToF detector (Table S2). Gaussians were fitted to the extracted ATDs using the 'Gaussian Fitting' module of CIUSuite 2 v2.2[40]. Gaussian fitting was performed in the protein only mode, with all signals considered to be related to the analyte. The following parameters were used for all ATDs: minimum peak amplitude = 0.05; maximum protein components fitted = 10; peak overlap penalty mode = relaxed, which penalizes overlaps > ~85%, but allows overlapping peaks to be chosen if other solutions are poorly fitted. Expected FWHMs were chosen based on the diffusion-limited formula $FWHM_{n\ passes} = FWHM_{1\ pass} \times \sqrt{n}$. This means that if for a given FWHM at 1 pass, the derived FWHM at 5 passes results in poor fitting (r^2 <0.98) or over-fitting (unrealistic number of features), then the FWHM at 1 pass needs to be adjusted. In our case, the expected FWHM for one population was estimated to be 2.0 ± 0.1 ms at 1 pass, corresponding to a value of 4.5 ± 0.1 ms at 5 passes. These values yield fits that are in good agreement with experimental data, *i.e.* r^2 >0.99.

CIU experiments. Collision voltages (CV) in the trap cell were increased from 0 to 200 V in 10 V steps. CIU data were processed using CIUSuite 2 v2.2[40]. ATDs were smoothed using a Savitsky-Golay algorithm (window length = 5 and polynomial order = 2). Acquisitions were performed in triplicate to generate average and differential RMSD plots. Interpolation by a factor 2 was used to double the number of points on the trap CV axis. For classification purposes, ATDs at trap 0 V were centered on the same drift time to achieve a comparison based solely on unfolding patterns, irrespective of drift time variations resulting from mass differences. Trastuzumab (IgG1), panitumumab (IgG2), and nivolumab (IgG4) were chosen as reference mAbs to build our classification method. Univariate feature selection (UFS) plots were used to select the most diagnostic voltages (*i.e.* with high discrimination scores) to identify subclasses of additional mAbs.

RESULTS

Does cIM-MS afford better separation of intact ~150 kDa mAbs?

We first compared IM/ATD profiles obtained on linear *versus* cyclic TWIMS cells to assess benefits of HR-IM-MS for the separation of native intact mAbs. Three different mAbs (elotuzumab – IgG1, panitumumab – IgG2, nivolumab – IgG4) serve as examples to illustrate cIM-MS capabilities (Figure 1A, B). Lower charge states are most likely to retain native structures and limit gas-phase collapse[5, 41-43], and so we decided to focus on the 27+ charge state, which offers a good compromise between IM-MS intensities (Table S3A) and "near-native" conformations.

On the linear platform, extracted ATDs overlap due to poor IM resolution, with only a small difference in drift times (Δt_D = 0.8 ms) between the highest-mobility (nivolumab) and lowest-mobility (panitumumab) mAbs (Figure 1C). On the cyclic instrument, a slight separation is already observed after one pass, and Δt_D between nivolumab and panitumumab increases to 1.9 ms. As prolonged exposure to T-waves does not alter the native conformation of proteins[27], multipass separation was used to take full advantage of cIM-MS capabilities. After five passes, the separation of nivolumab/panitumumab is further enhanced to 11.0 ms, resulting in clearly distinguished ATD apexes (Figure 1C). A wrap-around effect occurs beyond five passes with our parameters, meaning that high-mobility ions catch up with low-mobility ones, blurring the separation and avoiding additional passes for intact mAbs. Of note, significant ion losses (78 – 92%) happen after five passes for the 27+ charge state, which may be explained by diffusion and/or charge repulsion in the cIM racetrack (Table S3A).

Interestingly, ATDs broaden for all mAbs with increasing number of cIM passes, but without any improvement of resolution ($t_D/\Delta t_D$) between overlapping features, a time-based resolving power of ~16 being obtained after both one and five passes. These observations are in agreement with previously reported ones of reference native proteins: the theoretical 2.2× increase in resolution (corresponding to $\sqrt{n}$, where n is the number of passes) is not achieved after five passes because native ions possess multiple conformers that are difficult to decipher even with HR-IM-MS instruments[27-29, 44]. This is especially true for

mAbs, whose conformational spaces are richer than similarly-sized protein complexes due to their inherent flexibility[28, 43]. These results show that separating coexisting conformers for native proteins is still highly challenging, because of conformational heterogeneity, flexibility, or possible interconversion between species.

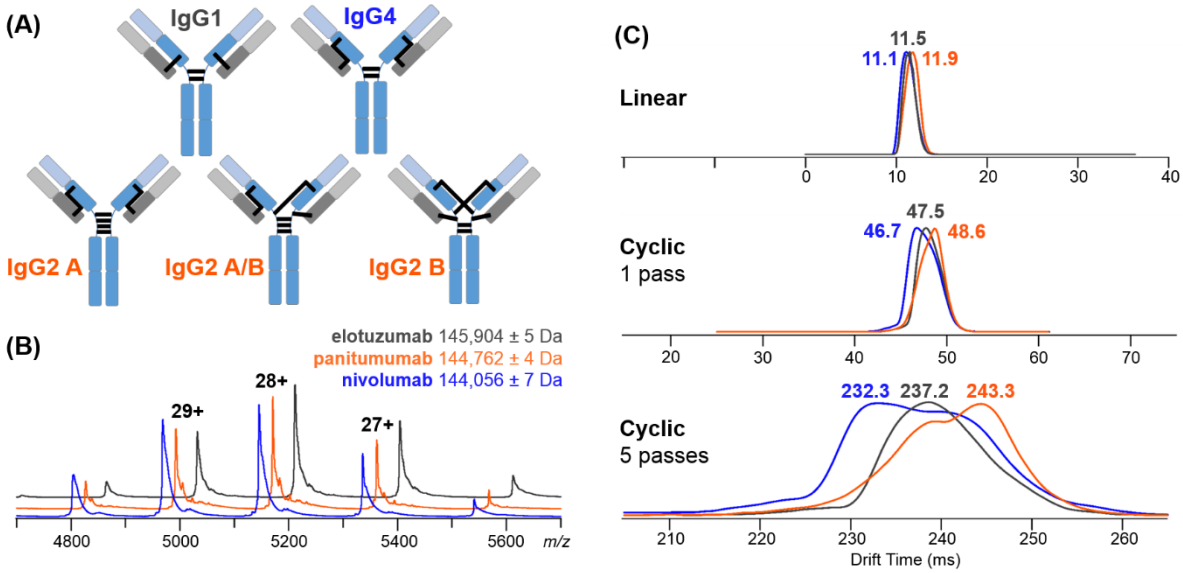

Figure 1. (A) Schematic representation of the three main IgG subclasses. Light and heavy chains are represented in grey and blue, respectively. Interchain disulfide bonds are depicted in black. **(B)** Native MS spectra of intact deglycosylated elotuzumab (grey), panitumumab (orange) and nivolumab (blue). **(C)** Extracted ATDs (z = 27+) obtained for the three mAbs using either a linear or a cyclic TWIMS cell after 1 and 5 passes.

Reproducibility of cIM behaviors for IgGs

As IM-based approaches are particularly well adapted for the characterization of proteins containing disulfide bonds, we took advantage of the diversity of mAb IgG-based formats (Figure 1A) as a fit for purpose application to illustrate the interest of IM-MS/CIU for this particular family of disulfide-rich proteins[20, 31, 37].

Gaussian fittings as a way of deciphering cIM-MS profiles – In order to provide a semi-quantitative interpretation of our HR-IM-MS data, Gaussian fits were used as a means to visualize the highly populated conformational landscapes of mAbs, aiming to (i) evaluate if HR-IM-MS can enhance the separation of multiple conformers, and (ii) provide a relative comparison between our samples. As Gaussian functions depend on estimated fitting parameters (see Materials and Methods for parameters' adjustment), fits are employed here in a differential manner for the direct comparison of samples. The number of fitted curves established after n passes does not absolutely represent the definitive "real" number of coexisting conformers. In the following paragraphs, we will only discuss the most significant Gaussians fits which are required to achieve r^2 >0.98. These features were reproducible for technical replicates (multiple measurements or preparations of the same sample, Table S4). We thus consider them as reliable metrics for mAbs' comparison purposes, contrary to minor species (*i.e.* relative intensity <20% in our case) that show more variability, are not always present in every technical replicate, and do not significantly contribute to r^2.

Intraclass variability – We first analyzed three IgG1 mAbs (trastuzumab, elotuzumab and ofatumumab, each encompassing eight intra- and four inter- chain disulfide bonds, see Figure 1A) to determine whether IM behaviors are similar across one subclass. For the 27+ charge state, a single IM peak (FWHM between 2.5 – 3.2 ms) is observed after one pass, with two major contributions detected by using Gaussian fitting (Figure 2A). Because of very close masses, the resolution at one pass is not sufficient to separate trastuzumab (145,903 ± 6 Da) and elotuzumab (145,911 ± 6 Da). Differences between trastuzumab and elotuzumab remain subtle even after five passes, but ofatumumab (146,540 ± 5 Da) could be slightly separated from the two other mAbs (Figure 2B). Peak broadening is also observed for all samples (FWHM = 12.7 – 12.9 ms) after five passes. Consequently, new conformational features are uncovered at five passes, with five main populations fitted for each IgG1 (Figure 2B, Table S4). It is important to note that for each mAb, cIM behaviors at one or five passes are reproducible based on the drift time of the most intense peak, the FWHM, and the asymmetry factor (Figure S1). For these three metrics, %RSDs between technical replicates are below values published by regulatory agencies (U.S. FDA)[45], thus enabling consistent mAb profiling with cIM-MS (Table S5). In particular, our dataset shows a low intra-IgG1 variability, with RMSDs <4% when comparing the cIM profiles of the three IgG1s at five passes (Figure S2A).

Similar conclusions can be drawn for IgG4 mAbs (nivolumab, reslizumab, natalizumab) (Figure 2C, D) that exhibit the same number of inter- and intra- chain disulfide bridges as IgG1s but with different connectivities. At one pass, a unique IM peak is observed (FWHM = 3.6 – 3.9 ms). ATDs broaden after five passes (FWHM = 17.6 – 18.5 ms) and six major Gaussian features are fitted for each IgG4. Interestingly, a slight double distribution starts appearing for nivolumab at five passes. Again, characteristics of cIM profiles are reproducible for all mAbs (Table S5). As for IgG1s, high intraclass similarities are evidenced by RMSDs <8% between the different IgG4s (Figure S2A).

Lastly, IgG2s appear ideally suited to assess the potential of cIM-MS, as they possess three hinge-related disulfide isoforms (A, A/B, and B, Figure 1A) that are most susceptible to be differentiated with high resolving powers. Both denosumab and eculizumab already present a bimodal distribution after one pass, and the separation of the two main peaks is enhanced after five passes (Figure 2E, F). For panitumumab, even if its asymmetry factor <1 indicates the presence of a left-side shoulder at one pass (Table S5A), multiple passes are required to evidence a bimodal ATD (Figure 2F). These two major conformational populations most likely stem from the presence of interchain disulfide isoforms that are specific to IgG2s. Our results are in agreement with those reported by Bagal *et al*.[38] and Jones *et al.*[46] who both observed that in most cases, only two disulfide isoforms are distinguished by native IM-MS.

Collectively, our experiments show that cIM behaviors of IgGs are reproducible for each sample, and even across each IgG subclass, allowing for robust mAb profiling with cIM-MS. HR-IM-MS provides first opportunities to decipher the rich conformational spaces of native mAbs thanks to the use of multipass separation. However, despite clear benefits of high IM resolution when disulfide variants are involved,

baseline-resolution is not achieved, evidencing some limitations of HR-IM-MS for native mAbs, again explained in part by their flexible nature.

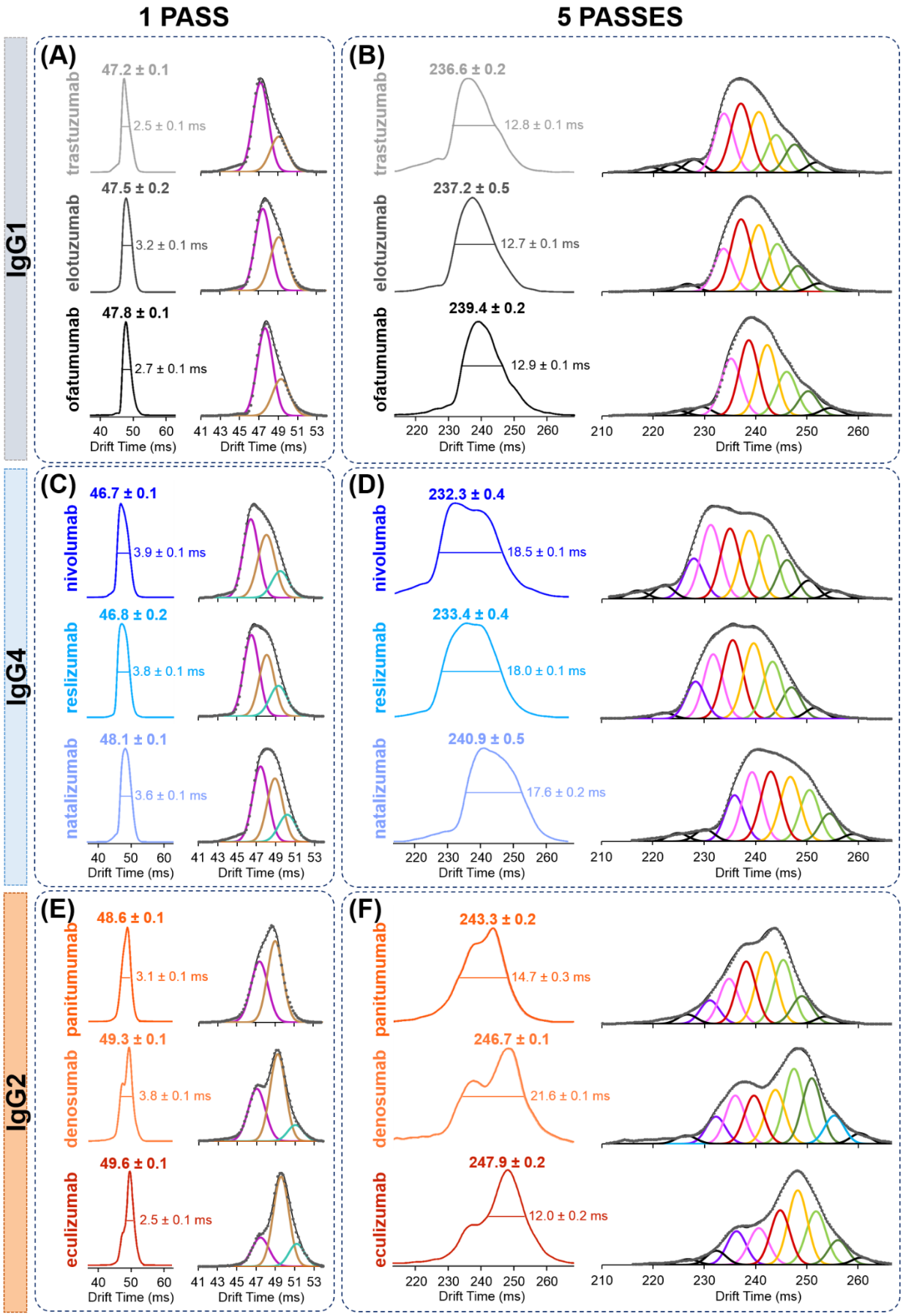

Figure 2. Extracted ATDs of IgGs after 1 or 5 passes on the cyclic instrument for charge state 27+. cIM profiles and their Gaussian fittings obtained for **(A, B)** three IgG1s, **(C, D)** three IgG4s, and **(E, F)** two IgG2s and an IgG2/4. Significant fits that are required to achieve r^2 >0.98 are colored and minor contributions are represented in black. Intensities of all ATDs are reported in Table S3A.

Benefits of cIM-MS for high-resolution CIU

CIU on linear versus cyclic TWIMS cells – In order to complement our IM-MS experiments, we next assessed the interest of combining HR-IM-MS to CIU approaches (CIU-cIM) to improve mAb fingerprinting. For CIU experiments, ions are activated in the trap cell located upstream of the cIM cell (Figure S3). CIU data generated after one pass on the cIM-MS instrument were then compared to those obtained using a linear TWIMS cell. Direct comparisons of transition voltages between both IM-MS devices are not relevant here as different geometries may induce variations in terms of CIU_{50} values. In addition, the background gas for collisions in the trap cell is argon on the linear instrument, which is more activating (higher polarizability) than nitrogen used on the cIM-MS platform[47, 48]. As collisions with argon are more energetic, unfolding transitions will occur at lower trap CVs on the linear TWIMS instrument.

CIU patterns of the most native charge states (*i.e.* lower charge states) are generally preferred for CIU analysis[31, 37], as Coulomb repulsions are minimized, and so we mainly focused on the 27+ charge state of intact mAbs, which offers the best compromise between "near-native" conformation, number of unfolding states, and signal intensity. For intact elotuzumab (IgG1), six features are detected with CIU-cIM (Figure 3A). States 1 and 2 (along with states 3 and 4) are now well defined (Δt_D = 2.5 ms) compared to CIU on the linear instrument, for which both conformers are comprised within a single broad ATD. Benefits of high-resolution CIU-cIM are even more evident for IgG4s. For intact nivolumab, six conformational states are observed on the cIM-MS instrument, while only four features could be seen on the CIU plot generated with linear TWIMS (Figure 3B). In particular, CIU-cIM reveals two coexisting features (3 and 4), with a corresponding separation of 19% valley, whereas the first-generation instrument does not differentiate the two conformers (Figure S4). Lastly, CIU plots are very similar for the IgG2 subclass with linear and cyclic TWIMS cells as illustrated on intact panitumumab (Figure 3C). IgG2s' unfolding patterns are generally less crowded than those of IgG1/4s, with fewer transitions due to increased stability conferred by additional disulfide bridges in the IgG2 hinge region[20, 31], which also explains well-resolved IgG2 CIU fingerprints on the linear TWIMS instrument. Of note, for panitumumab, the influence of the collision gas is well illustrated by the delayed appearance of state 3 on the cIM-MS platform compared to the linear device.

Interestingly, in our hands, CIU performances in terms of reproducibility and robustness are even better on the cyclic (RMSD between technical replicates ~4%) than on the linear TWIMS (~7%), compliant with U.S. FDA values (< 10%)[45].

Multipass CIU-cIM – To further explore the potential of multipass analysis for CIU fingerprinting, CIU plots were generated after two passes on the cIM-MS instrument for intact trastuzumab (IgG1). CIU plots for the 27+ charge state exhibit six conformational states like the one-pass fingerprint (Figure 3D). Although no additional features are uncovered, coexisting activated states are better separated as the IM resolving power increases. First, features are distributed over a larger drift time range after two passes, as the difference between drift times of the ground state (state 0) and the most unfolded one (state 5) increases to

32 ms, compared to Δ16 ms at one pass. As expected, the % valley separation also improves with the number of passes. At trap CV = 80 V, coexisting conformers are resolved at 57% of the valley after two passes, which represents an increase of +17% compared to one pass (Figure 3D). Similarly, a gain of +19% in valley separation is obtained between the main features present at trap CV = 180 V. Benefits of multipass CIU-cIM for enhanced graphical resolution of CIU fingerprints are well illustrated for intact trastuzumab, paving the way for better fingerprinting of mAbs directly at intact level.

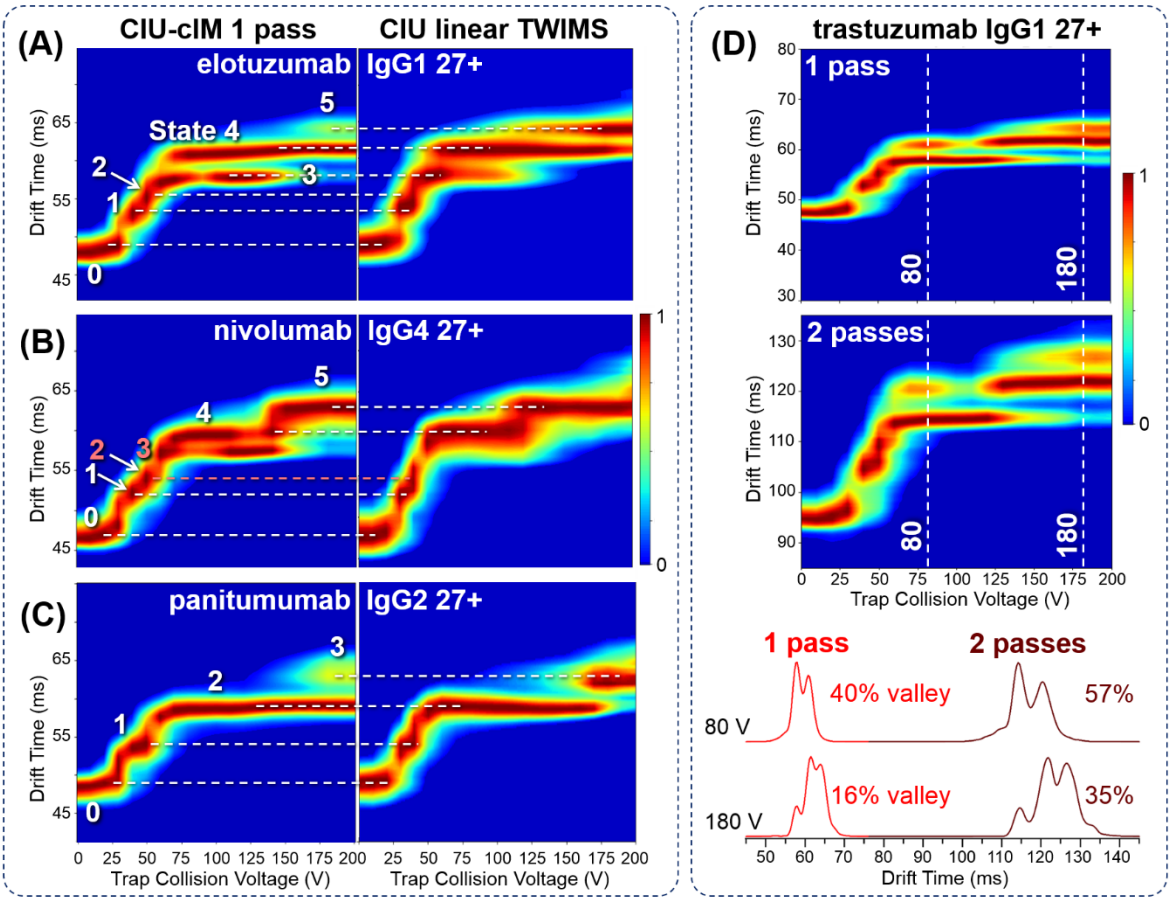

Figure 3. (A, B, C) Comparisons of fingerprints acquired on the cyclic (1 pass) *versus* linear TWIMS instrument, for intact deglycosylated elotuzumab, nivolumab and panitumumab. **(D)** CIU-cIM fingerprints generated for intact deglycosylated trastuzumab at one and two passes. ATDs were extracted at trap CV = 80 and 180 V, with associated % valley separation calculated between the two main features. Intensities of ATDs are reported in Table S3B.

Can cIM-MS and CIU-cIM distinguish IgG subclasses?

As already mentioned in previous sections, IgG subclasses possess specific interchain disulfide bridges and are expected to exhibit different IM and CIU behaviors. Therefore, benchmarking of IM-MS and CIU method developments for mAb analysis is often based on their ability to separate and distinguish IgG subclasses[49-51].

IM does not unambiguously distinguish IgG isotypes – While IM-MS has successfully pinpointed subtle changes in disulfide bridging of peptides[52-54] and small proteins[39], low-resolution TWIMS has failed to distinguish IgG subclasses in spite of their distinct disulfide patterns[20, 31]. In an attempt to identify the isotype of any canonical IgG directly based on its IM profile, we next assessed whether HR-IM-MS allows for the differentiation of IgGs 1, 2, and 4.

The first observation that stands out is that IgG2s exhibit a signature bimodal IM profile resulting from their specific disulfide isoforms, thus affording unequivocal differentiation from IgG1s and IgG4s. While IgG2s can be rapidly singled out, IgGs 1 and 4 both have four disulfide bonds, and only differ in terms of disulfide patterns. After one pass on the cIM-MS instrument, ATDs for IgG4s appear to be slightly broader (FWHM = 3.6 – 3.9 ms) than those of IgG1s (FWHM = 2.5 – 3.2 ms). This trend is further enhanced after five passes, as IgG4s present higher FWHM values than IgG1s (+5.2 ms on average), as reflected by the higher number of major conformers fitted for IgG4s compared to IgG1s (six *versus* five, respectively, Figure 2B, D). These observations indicate that IgG4s possess an increased gas-phase flexibility compared to IgG1s, which is in good agreement with trends underlined by Pacholarz *et al.*[43], who suggested that the light chain (Cys^{214}) being linked further from the center of mass on IgG4s compared to IgG1s (Cys^{131} *versus* Cys^{220} on the heavy chain) confers more movement to IgG4s (Figure 1A). Even if variations remain subtle between IgG1s/IgG4s, intraclass RMSDs are slightly higher (10 – 18 %) than interclass (2 – 8 %) or technical (< 2%) ones, with further points toward isotype-related IM behaviors (Figure S2A). Figure S2B shows the linear discriminants plot constructed based on ATDs at five passes, which groups IgG subclasses into well-separated clusters. The isotype of our test data was correctly assigned, showing it is possible to confirm the categorization of a sample with algorithm-aided workflows.

Overall, our results suggest that IgG1/IgG4 differentiation is not as obvious as IgG2 identification, but might be based on larger FWHMs observed for IgG4s, considering that similar trends are observed for charge state 28+ (Figure S5). At this stage and for fast and reliable isotype classification purposes, we must admit that strong expertise in data interpretation is still required to distinguish IgG1/4s in a straightforward manner based solely on cIM-MS profiles, in particular if no reference samples are available. It is worth noting that in a sample containing several mAbs from distinct subclasses, isotype identification may still be inferred from relative comparison of FWHMs, as illustrated by an elotuzumab (IgG1)/natalizumab (IgG4) mixture which yields similar cIM profiles than for the two separate mAbs (Figure S6A, B). However, for such mAb cocktails, species need to be first separated in the MS dimension to allow for ATD extraction of each mAb, or else only a single broad ATD will be obtained by IM. Adding an initial level of separation through the use of liquid chromatography (LC-IM-MS) could help to disentangle complex samples for individual mAb IM profiling.

CIU-cIM provides better differentiation of IgG subclasses – We finally evaluated the influence of CIU-cIM on intact 150 kDa IgG differentiation by using UFS plots[20, 40, 51]. For the 27+ charge state of intact mAbs, the UFS plot generated based on intact trastuzumab (IgG1), panitumumab (IgG2) and nivolumab (IgG4) clearly evidences advantages of CIU-cIM over CIU with linear TWIMS (Figure 4A). While the maximum $-\log_{10}$(p-value) value achieved on the linear instrument is ~0.9, CIU-cIM affords differentiation scores up to ~1.3. cIM also yields lower standard deviations than the linear TWIMS, especially between 50 – 100 V, in agreement with previous observations on RMSD values between technical replicates. These results are even

more obvious for the 28+ charge state (Figure 4B, see Figure S7 for 28+ CIU fingerprints): the most discriminating region identified for CIU-cIM ranges from 100 to 140 V, with nine CVs whose $-\log_{10}$(p-value) values are all greater than the best score that could be reached with linear TWIMS (~0.7). These data definitely illustrate how increased IM resolution contributes to an easier differentiation of IgG subclasses. Overall, a broader range of diagnostic CVs with higher differentiation scores is available in CIU-cIM, leading to more accurate categorization of IgG subclasses, as exemplified by the 27+ charge state of intact IgG1 elotuzumab (Figure 4C). On the linear TWIMS, elotuzumab is recognized as an IgG1 (59.7 ± 2.7%), even if the IgG4 isotype cannot be unambiguously ruled out (34.3 ± 2.4%), showing once again how the distinction of IgG1/4 can be challenging at the intact level with a low IM resolution. Conversely, scores of 87.3 ± 1.5% are obtained using cIM, allowing for unambiguous IgG1 identification at the intact level. Our classification method was further applied to a series of intact mAbs belonging to different IgG subclasses (Figure S7). Denosumab was categorized as an IgG2 with an excellent score of 99.4 ± 0.7%, corroborating the fact that IgG2s exhibit a distinct behavior compared to other subclasses offering unequivocal classification. Ofatumumab and natalizumab were successfully clusterized as IgG1 (90.6 ± 3.1%) and IgG4 (84.8 ± 5.1%), respectively. Similar scores were obtained for the 28+ charge state (Figure S7).

To conclude, CIU fingerprinting gives stronger confidence in the determination of IgG isotypes compared to HR-IM-MS profiles, especially for IgGs 1 *versus* 4. Although it could be argued that CIU experiments are longer than IM-MS measurements, we were also able to achieve high categorization scores by performing targeted-scheduled multiplexed CIU-cIM that we previously developed on the linear TWIMS instrument[51] (Figure S6C). This leads to drastic time reduction (~15 min for two mAbs) for CIU data collection while ensuring precise subtype identification, and can thus represent an attractive alternative to clarify ambiguous IM-MS results.

These experiments demonstrate that the use of HR-CIU combined to automated classification tools offers a clear-cut and straightforward classification of all mAbs directly at intact level, with scores >85%, which was not possible at the intact level on linear IM-MS instrument.

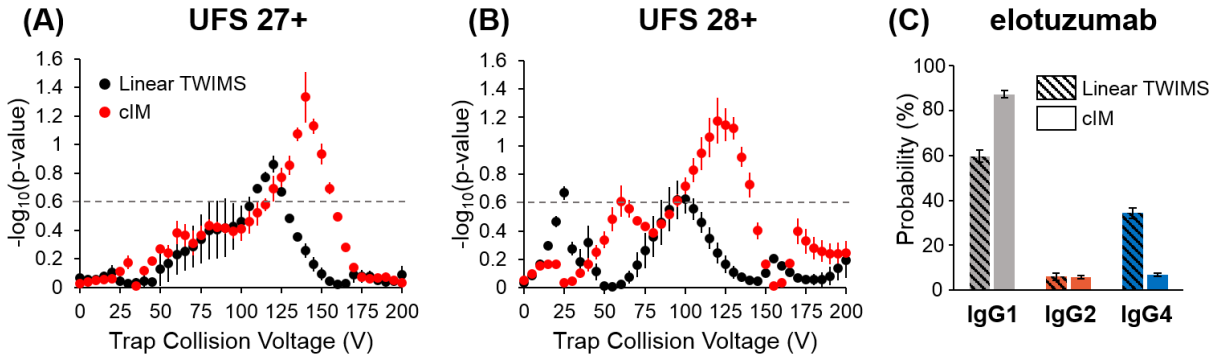

Figure 4. Differentiation of IgG subclasses based on CIU behaviors. (A, B) UFS plots generated with the linear (black) and cyclic (red) instruments for charge states 27+ and 28+. Trastuzumab (IgG1), panitumumab (IgG2) and nivolumab (IgG4) were used as reference mAbs to build the classification method. **(C)** Subclassification scores for each IgG isotype obtained on both platforms in the case of intact deglycosylated elotuzumab (IgG1). Subclassification was performed on charge state 27+ using trap CVs 125 to 155 (in 5 V steps).

CONCLUSIONS

The present work aimed at providing a first panoramic overview of the capabilities of a HR-IM-MS instrument based on cyclic TWIMS technology for the conformational characterization of mAbs. As the use of IM-MS is still scarce in biopharmaceutical industries, hopes are pinned on second-generation HR-IM-MS instruments. For biopharmaceutical applications, IM-MS can be envisioned in several ways ranging from simple qualitative ATD/IM study, to the use of accurate CCS values as descriptors of mAb conformations (as implemented for small molecules analysis), or even through comparison of mAbs' fingerprints obtained after activation.

We demonstrated that cIM-MS generates highly reproducible datasets for both IM and CIU plots, affording robust profiling and fingerprinting. However, it is clear that the impact of HR-IM-MS (without activation, *e.g.* comparison of ATD profiles or drift times, CCS measurements) is still limited for intact native mAbs, as opposed to smaller molecules for which HR-IM-MS constitutes a real breakthrough[26]. mAbs represent particularly challenging systems both in terms of size and flexibility. They adopt a whole range of conformations, leading to a quasi-continuous range of CCSs, which at this stage cannot be individually resolved. Even if higher accessible resolving powers afford first progress compared to early-generation instruments, baseline-separation is still far from being achieved. Nonetheless, we showed that multipass IM was able to distinguish disulfide isoforms of IgG2s. Conversely, when moving to activation methods such as CIU experiments, cIM-MS clearly outperforms the linear TWIMS technology, providing HR graphical fingerprints with a better separation of features along with uncovering of additional conformational states. For classification purposes, differences between ATDs of IgGs 1 and 4 were subtle, and rely on IM-peak broadening of IgG4s related to their higher flexibility, thus still requiring strong expertise in data interpretation. Conversely, CIU-cIM approaches unambiguously distinguish all IgG subclasses at the intact level, which represents a clear improvement over linear TWIMS CIU analysis. In previous studies, we showed that CIU fingerprints on linear TWIMS instruments provide straightforward IgG categorization only if classification is performed on downsized mAbs digested into subunits (middle-up level)[20, 31], and not on intact mAbs. Here, we provided definitive proof that CIU-based classification is ready to use directly at the intact level on cIM-MS platforms in biopharmaceutical companies. Full range or even higher throughput targeted-scheduled-CIU analyses afford specific isotype signature of any mAb within ~15 min experiment without extensive sample preparation (enzymatic digestion). Even if multipass experiments seem appealing to generate HR-CIU fingerprints, data recording remains challenging and may be hampered by misdetection of unfolded states generated at high activation energies, and possible wrap-around, which both limit possibilities for multipass CIU. In order to ease data collection and treatment, we advise to acquire CIU fingerprints at one pass, which is already enough to achieve significant improvements over linear TWIMS instruments.

Several alternatives can be envisioned to overcome hurdles related to the dynamic nature of mAbs that limits IM resolution. First, we expect that more sophisticated multifunction capabilities available on the cIM-MS platform and not investigated in the present work, such as slicing[35] and isolation that can even be applied to CIU experiments[55], will improve the differentiation of coexisting populations by focusing on narrow regions of an ATD that then undergo further IM separation. Slicing experiments could be performed to tackle interconversion events that most likely also contribute to the complexity of mAbs' IM profiles[35]. Isolation can also help to circumvent wrap-around by "trimming" IM windows[26]. As the spatial width of the ATD is reduced, it is then possible to do more passes around the cIM cell.

Next, as cIM operates in the millisecond timescale, it can be integrated into LC-MS couplings. The addition of an LC dimension is of interest to simplify ATDs and provide a first separation of conformers, especially by using ion exchange chromatography (IEX) which is able to separate charge variants (*e.g.* deamidation, isoAsp, oxidation, etc.)[56]. IEX is particularly attractive to study co-formulated antibodies as mAbs are differentiated based on their pIs[57], thus affording extraction of each separate ATD. Although less selective than IEX, other nondenaturing LC methods such as size exclusion chromatography (SEC) and hydrophobic interaction chromatography (HIC) can also be implemented for LC-IM-MS couplings[58, 59].

Finally, other HR-IM-MS instruments (TIMS, and SLIM who has limited ion losses and whose drift path is significantly longer than cIM) released in recent years may provide a better resolution of coexisting conformers for native intact mAbs. In particular, multipass ultra-long serpentine SLIM[24] or multilevel SLIM[60] designs allow for ions to drift on longer paths, thus reducing wrap-around phenomena. At present, reports on the characterization of large native assemblies on these two platforms are still scarce[28, 44].

To conclude, we reported here on the advantages and limitations of cIM-MS to tackle the rich conformational landscapes of mAbs. Even if there is still room for improvement, HR-IM-MS/CIU has the potential to address conformational heterogeneity that could arise from the increasing complexity of innovative mAb formats, as exemplified by the separation of conformational isomers of a trispecific antibody[61]. The cIM technology thus opens doors for HR IM-MS/CIU to support mAb development, and could undoubtedly be extended to the study of large protein complexes (even megadalton assemblies[62]) that are less flexible than antibodies.

ASSOCIATED CONTENT

Supporting Information

The Supporting Information is available free of charge on the ACS Publications website.

Voltages used to set the direction of the ions in the multifunction array region of cIM-MS spectrometer for each type of cIM event (Table S1); Determination of correction factors to derive drift times from raw arrival times (Table S2); Intensities obtained on the cIM-MS instrument for extracted ATDs (Table S3); Reproducibility of Gaussian fittings (Table S4); %RSDs between technical replicates of mAbs at 1 and 5 passes

on the cIM-MS instrument (Table S5); Parameters used to evaluate the reproducibility of cIM profiles (Figure S1); Intra- and interclass variations (Figure S2); Principle of CIU experiments performed in the trap cell of the cIM-MS instrument (Figure S3); Comparison of CIU plots obtained for intact deglycosylated nivolumab using a linear *versus* cyclic TWIMS cell (Figure S4); cIM-MS experiments for charge state 28+ after 4 passes (Figure S5); Analysis of a mixture containing two different mAbs on the cIM-MS instrument, including targeted scheduled CIU subclassification (Figure S6); CIU fingerprints and IgG classification scores for charge states 27 and 28+ (Figure S7) (PDF)

AUTHOR INFORMATION

Corresponding Author

*Sarah Cianférani. Phone : +33 (0)3 68 85 26 79 ; Email: sarah.cianferani@unistra.fr; Fax: +33 (0)3 68 85 27 81

Author Contributions

¶E.D. and S.O. contributed equally.

Notes

The authors declare no competing financial interest.

ACKNOWLEDGMENTS

This work was supported by the CNRS, the University of Strasbourg, the “Agence Nationale de la Recherche”, and the French Proteomic Infrastructure (ProFI; grant ANR-10-INBS-08-03). The authors would like to thank GIS IBiSA and Région Grand Est for financial support in purchasing a Synapt G2 HDMS instrument, as well as GIS IBiSA, Nantes Métropole, Région Pays-de-la-Loire and FEDER for financial support in purchasing a SELECT SERIES Cyclic IMS instrument. E.D. and S.O. acknowledge the French Ministry for Education and Research, and the “Agence Nationale de la Recherche” (grant ANR-18-CE29-0006), respectively, for funding of their Ph.D.

REFERENCES

(1) Kaplon, H.; Chenoweth, A.; Crescioli, S.; Reichert, J. M., Antibodies to watch in 2022. *MAbs* **2022,** *14* (1), 2014296.

(2) Vidarsson, G.; Dekkers, G.; Rispens, T., IgG Subclasses and Allotypes: From Structure to Effector Functions. *Front Immunol* **2014,** *5*.

(3) Xu, Y.; Wang, D.; Mason, B.; Rossomando, T.; Li, N.; Liu, D.; Cheung, J. K.; Xu, W.; Raghava, S.; Katiyar, A.; Nowak, C.; Xiang, T.; Dong, D. D.; Sun, J.; Beck, A.; Liu, H., Structure, heterogeneity and developability assessment of therapeutic antibodies. *mAbs* **2018,** *11* (2), 239-264.

(4) Terral, G.; Beck, A.; Cianférani, S., Insights from native mass spectrometry and ion mobility-mass spectrometry for antibody and antibody-based product characterization. *J Chromatogr B: Anal Technol Biomed Life Sci* **2016,** *1032*, 79-90.

(5) Campuzano, I. D. G.; Larriba, C.; Bagal, D.; Schnier, P. D., *Ion Mobility and Mass Spectrometry Measurements of the Humanized IgGk NIST Monoclonal Antibody*. 2015; Vol. 1202, p 75-112.

(6) Upton, R.; Migas, L. G.; Pacholarz, K. J.; Beniston, R. G.; Estdale, S.; Firth, D.; Barran, P. E., Hybrid mass spectrometry methods reveal lot-to-lot differences and delineate the effects of glycosylation on the tertiary structure of Herceptin®. *Chem Sci* **2019,** *10* (9), 2811-2820.
(7) Debaene, F.; Wagner-Rousset, E.; Colas, O.; Ayoub, D.; Corvaïa, N.; Van Dorsselaer, A.; Beck, A.; Cianférani, S., Time Resolved Native Ion-Mobility Mass Spectrometry to Monitor Dynamics of IgG4 Fab Arm Exchange and "Bispecific" Monoclonal Antibody Formation. *Anal Chem* **2013,** *85* (20), 9785-9792.
(8) Vallejo, D. D.; Jeon, C. K.; Parson, K. F.; Herderschee, H. R.; Eschweiler, J. D.; Filoti, D. I.; Ruotolo, B. T., Ion Mobility–Mass Spectrometry Reveals the Structures and Stabilities of Biotherapeutic Antibody Aggregates. *Anal Chem* **2022,** *94* (18), 6745-6753.
(9) Debaene, F.; Bœuf, A.; Wagner-Rousset, E.; Colas, O.; Ayoub, D.; Corvaïa, N.; Van Dorsselaer, A.; Beck, A.; Cianférani, S., Innovative Native MS Methodologies for Antibody Drug Conjugate Characterization: High Resolution Native MS and IM-MS for Average DAR and DAR Distribution Assessment. *Anal Chem* **2014,** *86* (21), 10674-10683.
(10) Marcoux, J.; Champion, T.; Colas, O.; Wagner-Rousset, E.; Corvaia, N.; Van Dorsselaer, A.; Beck, A.; Cianferani, S., Native mass spectrometry and ion mobility characterization of trastuzumab emtansine, a lysine-linked antibody drug conjugate. *Protein Sci* **2015,** *24* (8), 1210-1223.
(11) Botzanowski, T.; Erb, S.; Hernandez-Alba, O.; Ehkirch, A.; Colas, O.; Wagner-Rousset, E.; Rabuka, D.; Beck, A.; Drake, P. M.; Cianferani, S., Insights from native mass spectrometry approaches for top- and middle- level characterization of site-specific antibody-drug conjugates. *mAbs* **2017,** *9* (5), 801-811.
(12) Campuzano, I. D. G.; Lippens, J. L., Ion mobility in the pharmaceutical industry: an established biophysical technique or still niche? *Curr Opin Chem Biol* **2018,** *42*, 147-159.
(13) Roux, K. H.; Strelets, L.; Michaelsen, T. E., Flexibility of human IgG subclasses. *J Immunol* **1997,** *159* (7), 3372-82.
(14) Guddat, L. W.; Herron, J. N.; Edmundson, A. B., Three-dimensional structure of a human immunoglobulin with a hinge deletion. *Proc Natl Acad Sci U S A* **1993,** *90* (9), 4271-5.
(15) Harris, L. J.; Larson, S. B.; Hasel, K. W.; McPherson, A., Refined structure of an intact IgG2a monoclonal antibody. *Biochemistry* **1997,** *36* (7), 1581-97.
(16) Harris, L. J.; Skaletsky, E.; McPherson, A., Crystallographic structure of an intact IgG1 monoclonal antibody. *J Mol Biol* **1998,** *275* (5), 861-72.
(17) Saphire, E. O.; Parren, P. W.; Pantophlet, R.; Zwick, M. B.; Morris, G. M.; Rudd, P. M.; Dwek, R. A.; Stanfield, R. L.; Burton, D. R.; Wilson, I. A., Crystal Structure of a Neutralizing Human IgG Against HIV-1: A Template for Vaccine Design. *Science* **2001,** *293* (5532), 1155-1159.
(18) Scapin, G.; Yang, X.; Prosise, W. W.; McCoy, M.; Reichert, P.; Johnston, J. M.; Kashi, R. S.; Strickland, C., Structure of full-length human anti-PD1 therapeutic IgG4 antibody pembrolizumab. *Nat Struct Mol Biol* **2015,** *22* (12), 953-958.
(19) Hernandez-Alba, O.; Wagner-Rousset, E.; Beck, A.; Cianferani, S., Native Mass Spectrometry, Ion Mobility, and Collision-Induced Unfolding for Conformational Characterization of IgG4 Monoclonal Antibodies. *Anal Chem* **2018,** *90* (15), 8865-8872.
(20) Botzanowski, T.; Hernandez-Alba, O.; Malissard, M.; Wagner-Rousset, E.; Deslignière, E.; Colas, O.; Haeuw, J.-F.; Beck, A.; Cianférani, S., Middle level IM-MS and CIU experiments for improved therapeutic immunoglobulin subclass fingerprinting. *Anal Chem* **2020,** *92* (13), 8827-8835.
(21) Pacholarz, K. J.; Peters, S. J.; Garlish, R. A.; Henry, A. J.; Taylor, R. J.; Humphreys, D. P.; Barran, P. E., Molecular Insights into the Thermal Stability of mAbs with Variable-Temperature Ion-Mobility Mass Spectrometry. *Chembiochem* **2016,** *17* (1), 46-51.
(22) Norgate, E. L.; Upton, R.; Hansen, K.; Bellina, B.; Brookes, C.; Politis, A.; Barran, P. E., Cold Denaturation of Proteins in the Absence of Solvent: Implications for Protein Storage. *Angew Chem Int Ed Engl* **2022**.
(23) Pringle, S. D.; Giles, K.; Wildgoose, J. L.; Williams, J. P.; Slade, S. E.; Thalassinos, K.; Bateman, R. H.; Bowers, M. T.; Scrivens, J. H., An investigation of the mobility separation of some peptide and protein ions using a new hybrid quadrupole/travelling wave IMS/oa-ToF instrument. *Int J Mass Spectrom* **2007,** *261* (1), 1-12.
(24) Deng, L.; Webb, I. K.; Garimella, S. V. B.; Hamid, A. M.; Zheng, X.; Norheim, R. V.; Prost, S. A.; Anderson, G. A.; Sandoval, J. A.; Baker, E. S.; Ibrahim, Y. M.; Smith, R. D., Serpentine Ultralong Path with

Extended Routing (SUPER) High Resolution Traveling Wave Ion Mobility-MS using Structures for Lossless Ion Manipulations. *Anal Chem* **2017,** *89* (8), 4628-4634.
(25) Adams, K. J.; Montero, D.; Aga, D.; Fernandez-Lima, F., Isomer separation of polybrominated diphenyl ether metabolites using nanoESI-TIMS-MS. *Int J Ion Mobility Spectrom* **2016,** *19* (2-3), 69-76.
(26) Giles, K.; Ujma, J.; Wildgoose, J.; Pringle, S.; Richardson, K.; Langridge, D.; Green, M., A Cyclic Ion Mobility-Mass Spectrometry System. *Anal Chem* **2019,** *91* (13), 8564-8573.
(27) Eldrid, C.; Ujma, J.; Kalfas, S.; Tomczyk, N.; Giles, K.; Morris, M.; Thalassinos, K., Gas Phase Stability of Protein Ions in a Cyclic Ion Mobility Spectrometry Traveling Wave Device. *Anal Chem* **2019,** *91* (12), 7554-7561.
(28) Jeanne Dit Fouque, K.; Garabedian, A.; Leng, F.; Tse-Dinh, Y.-C.; Ridgeway, M. E.; Park, M. A.; Fernandez-Lima, F., Trapped Ion Mobility Spectrometry of Native Macromolecular Assemblies. *Anal Chem* **2021,** *93* (5), 2933-2941.
(29) Snyder, D. T.; Jones, B. J.; Lin, Y.-F.; Cooper-Shepherd, D. A.; Hewitt, D.; Wildgoose, J.; Brown, J. M.; Langridge, J. I.; Wysocki, V. H., Surface-induced dissociation of protein complexes on a cyclic ion mobility spectrometer. *The Analyst* **2021,** *146* (22), 6861-6873.
(30) Dixit, S. M.; Polasky, D. A.; Ruotolo, B. T., Collision induced unfolding of isolated proteins in the gas phase: past, present, and future. *Curr Opin Chem Biol* **2018,** *42*, 93-100.
(31) Tian, Y.; Han, L.; Buckner, A. C.; Ruotolo, B. T., Collision Induced Unfolding of Intact Antibodies: Rapid Characterization of Disulfide Bonding Patterns, Glycosylation, and Structures. *Anal Chem* **2015,** *87* (22), 11509-11515.
(32) Pisupati, K.; Tian, Y.; Okbazghi, S.; Benet, A.; Ackermann, R.; Ford, M.; Saveliev, S.; Hosfield, C. M.; Urh, M.; Carlson, E.; Becker, C.; Tolbert, T. J.; Schwendeman, S. P.; Ruotolo, B. T.; Schwendeman, A., A Multidimensional Analytical Comparison of Remicade and the Biosimilar Remsima. *Anal Chem* **2017,** *89* (9), 4838-4846.
(33) Desligniere, E.; Ehkirch, A.; Duivelshof, B. L.; Toftevall, H.; Sjogren, J.; Guillarme, D.; D'Atri, V.; Beck, A.; Hernandez-Alba, O.; Cianferani, S., State-of-the-Art Native Mass Spectrometry and Ion Mobility Methods to Monitor Homogeneous Site-Specific Antibody-Drug Conjugates Synthesis. *Pharmaceuticals (Basel)* **2021,** *14* (6).
(34) Watanabe, Y.; Vasiljevic, S.; Allen, J. D.; Seabright, G. E.; Duyvesteyn, H. M. E.; Doores, K. J.; Crispin, M.; Struwe, W. B., Signature of Antibody Domain Exchange by Native Mass Spectrometry and Collision-Induced Unfolding. *Anal Chem* **2018,** *90* (12), 7325-7331.
(35) Deslignière, E.; Ollivier, S.; Ehkirch, A.; Martelet, A.; Ropartz, D.; Lechat, N.; Hernandez-Alba, O.; Menet, J.-M.; Clavier, S.; Rogniaux, H.; Genet, B.; Cianférani, S., Combination of IM-Based Approaches to Unravel the Coexistence of Two Conformers on a Therapeutic Multispecific mAb. *Anal Chem* **2022,** *94* (22), 7981-7989.
(36) Hartmann, L.; Botzanowski, T.; Galibert, M.; Jullian, M.; Chabrol, E.; Zeder-Lutz, G.; Kugler, V.; Stojko, J.; Strub, J. M.; Ferry, G.; Frankiewicz, L.; Puget, K.; Wagner, R.; Cianférani, S.; Boutin, J. A., VHH characterization. Comparison of recombinant with chemically synthesized anti-HER2 VHH. *Protein Sci* **2019,** *28* (10), 1865-1879.
(37) Yin, Z.; Du, M.; Chen, D.; Zhang, W.; Huang, W.; Wu, X.; Yan, S., Rapid structural discrimination of IgG antibodies by multicharge-state collision-induced unfolding. *RSC Advances* **2021,** *11* (58), 36502-36510.
(38) Bagal, D.; Valliere-Douglass, J. F.; Balland, A.; Schnier, P. D., Resolving Disulfide Structural Isoforms of IgG2 Monoclonal Antibodies by Ion Mobility Mass Spectrometry. *Anal Chem* **2010,** *82* (16), 6751-6755.
(39) Atmanene, C. d.; Wagner-Rousset, E.; Malissard, M.; Chol, B.; Robert, A.; Corvaïa, N.; Dorsselaer, A. V.; Beck, A.; Sanglier-Cianférani, S., Extending Mass Spectrometry Contribution to Therapeutic Monoclonal Antibody Lead Optimization: Characterization of Immune Complexes Using Noncovalent ESI-MS. *Anal Chem* **2009,** *81* (15), 6364-6373.
(40) Polasky, D. A.; Dixit, S. M.; Fantin, S. M.; Ruotolo, B. T., CIUSuite 2: Next-Generation Software for the Analysis of Gas-Phase Protein Unfolding Data. *Anal Chem* **2019,** *91* (4), 3147-3155.
(41) Ruotolo, B. T.; Kevin, G.; Campuzano, I.; Sandercock, A. M.; Bateman, R. H.; Robinson, C. V., Evidence for Macromolecular Protein Rings in the Absence of Bulk Water. *Science* **2005,** *310* (5754), 1658-1661.

(42) Devine, P. W. A.; Fisher, H. C.; Calabrese, A. N.; Whelan, F.; Higazi, D. R.; Potts, J. R.; Lowe, D. C.; Radford, S. E.; Ashcroft, A. E., Investigating the Structural Compaction of Biomolecules Upon Transition to the Gas-Phase Using ESI-TWIMS-MS. *J Am Soc Mass Spectrom* **2017,** *28* (9), 1855-1862.
(43) Pacholarz, K. J.; Porrini, M.; Garlish, R. A.; Burnley, R. J.; Taylor, R. J.; Henry, A. J.; Barran, P. E., Dynamics of Intact Immunoglobulin G Explored by Drift-Tube Ion-Mobility Mass Spectrometry and Molecular Modeling. *Angew Chem Int Ed* **2014,** *53* (30), 7765-7769.
(44) Allen, S. J.; Eaton, R. M.; Bush, M. F., Analysis of Native-Like Ions Using Structures for Lossless Ion Manipulations. *Anal Chem* **2016,** *88* (18), 9118-9126.
(45) Ferguson, C. N.; Gucinski-Ruth, A. C., Evaluation of Ion Mobility-Mass Spectrometry for Comparative Analysis of Monoclonal Antibodies. *J Am Soc Mass Spectrom* **2016,** *27* (5), 822-833.
(46) Jones, L. M.; Zhang, H.; Cui, W.; Kumar, S.; Sperry, J. B.; Carroll, J. A.; Gross, M. L., Complementary MS Methods Assist Conformational Characterization of Antibodies with Altered S–S Bonding Networks. *J Am Soc Mass Spectrom* **2013,** *24* (6), 835-845.
(47) Morris, C. B.; May, J. C.; Leaptrot, K. L.; McLean, J. A., Evaluating Separation Selectivity and Collision Cross Section Measurement Reproducibility in Helium, Nitrogen, Argon, and Carbon Dioxide Drift Gases for Drift Tube Ion Mobility–Mass Spectrometry. *J Am Soc Mass Spectrom* **2019,** *30* (6), 1059-1068.
(48) Gabelica, V.; Marklund, E., Fundamentals of ion mobility spectrometry. *Curr Opin Chem Biol* **2018,** *42*, 51-59.
(49) Vallejo, D. D.; Polasky, D. A.; Kurulugama, R. T.; Eschweiler, J. D.; Fjeldsted, J. C.; Ruotolo, B. T., A Modified Drift Tube Ion Mobility-Mass Spectrometer for Charge-Multiplexed Collision-Induced Unfolding. *Anal Chem* **2019,** *91* (13), 8137-8146.
(50) Polasky, D. A.; Dixit, S. M.; Vallejo, D. D.; Kulju, K. D.; Ruotolo, B. T., An Algorithm for Building Multi-State Classifiers Based on Collision-Induced Unfolding Data. *Anal Chem* **2019,** *91* (16), 10407-10412.
(51) Deslignière, E.; Ehkirch, A.; Botzanowski, T.; Beck, A.; Hernandez-Alba, O.; Cianférani, S., Toward Automation of Collision-Induced Unfolding Experiments through Online Size Exclusion Chromatography Coupled to Native Mass Spectrometry. *Anal Chem* **2020,** *92* (19), 12900-12908.
(52) Massonnet, P.; Haler, J. R.; Upert, G.; Degueldre, M.; Morsa, D.; Smargiasso, N.; Mourier, G.; Gilles, N.; Quinton, L.; De Pauw, E., Ion Mobility-Mass Spectrometry as a Tool for the Structural Characterization of Peptides Bearing Intramolecular Disulfide Bond(s). *J Am Soc Mass Spectrom* **2016,** *27* (10), 1637-1646.
(53) Schmitz, T.; Pengelley, S.; Belau, E.; Suckau, D.; Imhof, D., LC-Trapped Ion Mobility Spectrometry-TOF MS Differentiation of 2- and 3-Disulfide-Bonded Isomers of the μ-Conotoxin PIIIA. *Anal Chem* **2020,** *92* (16), 10920-10924.
(54) Desligniere, E.; Botzanowski, T.; Diemer, H.; Cooper-Shepherd, D. A.; Wagner-Rousset, E.; Colas, O.; Bechade, G.; Giles, K.; Hernandez-Alba, O.; Beck, A.; Cianferani, S., High-Resolution IMS-MS to Assign Additional Disulfide Bridge Pairing in Complementarity-Determining Regions of an IgG4 Monoclonal Antibody. *J Am Soc Mass Spectrom* **2021,** *32* (10), 2505-2512.
(55) Eldrid, C.; Ben-Younis, A.; Ujma, J.; Britt, H.; Cragnolini, T.; Kalfas, S.; Cooper-Shepherd, D.; Tomczyk, N.; Giles, K.; Morris, M.; Akter, R.; Raleigh, D.; Thalassinos, K., Cyclic Ion Mobility–Collision Activation Experiments Elucidate Protein Behavior in the Gas Phase. *J Am Soc Mass Spectrom* **2021,** *32* (6), 1545-1552.
(56) Murisier, A.; Andrie, M.; Fekete, S.; Lauber, M.; D'Atri, V.; Iwan, K.; Guillarme, D., Direct coupling of size exclusion chromatography and mass spectrometry for the characterization of complex monoclonal antibody products. *J Sep Sci* **2022,** *45* (12), 1997-2007.
(57) Kim, J.; Kim, Y. J.; Cao, M.; De Mel, N.; Albarghouthi, M.; Miller, K.; Bee, J. S.; Wang, J.; Wang, X., Analytical characterization of coformulated antibodies as combination therapy. *mAbs* **2020,** *12* (1), 1738691.
(58) Ehkirch, A.; Hernandez-Alba, O.; Colas, O.; Beck, A.; Guillarme, D.; Cianferani, S., Hyphenation of size exclusion chromatography to native ion mobility mass spectrometry for the analytical characterization of therapeutic antibodies and related products. *J Chromatogr B: Anal Technol Biomed Life Sci* **2018,** *1086*, 176-183.
(59) Ehkirch, A.; D'Atri, V.; Rouviere, F.; Hernandez-Alba, O.; Goyon, A.; Colas, O.; Sarrut, M.; Beck, A.; Guillarme, D.; Heinisch, S.; Cianferani, S., An Online Four-Dimensional HIC×SEC-IM×MS Methodology for Proof-of-Concept Characterization of Antibody Drug Conjugates. *Anal Chem* **2018,** *90* (3), 1578-1586.
(60) Hollerbach, A. L.; Li, A.; Prabhakaran, A.; Nagy, G.; Harrilal, C. P.; Conant, C. R.; Norheim, R. V.; Schimelfenig, C. E.; Anderson, G. A.; Garimella, S. V. B.; Smith, R. D.; Ibrahim, Y. M., Ultra-High-Resolution

Ion Mobility Separations Over Extended Path Lengths and Mobility Ranges Achieved using a Multilevel Structures for Lossless Ion Manipulations Module. *Anal Chem* **2020,** *92* (11), 7972-7979.
(61) Mullard, A., FDA approves 100th monoclonal antibody product. *Nat Rev Drug Discovery* **2021,** *20* (7), 491-495.
(62) Harrison, J. A.; Pruška, A.; Bittner, P.; Muck, A.; Cooper-Shepherd, D. A.; Zenobi, R., Advancing Cyclic Ion Mobility Mass Spectrometry Methods for Studying Biomolecules: Toward the Conformational Dynamics of Mega Dalton Protein Aggregates. *Anal Chem* **2022,** *94* (36), 12435-12443.

Table of Contents graphic